Biosensors and Bioelectronics 59 (2014) 21–27

Contents lists available at ScienceDirect

Biosensors and Bioelectronics

journal homepage: www.elsevier.com/locate/bios

Ultrasensitive photoelectrochemical immunoassay of antibody against tumor-associated carbohydrate antigen amplified by functionalized graphene derivates and enzymatic biocatalytic precipitation

Xiaoru Zhang *, Mingshuai Liu, Yaning Mao, Yunpeng Xu, Shuyan Niu *

Key Laboratory of Sensor Analysis of Tumor Marker, Ministry of Education, College of Chemistry and Molecular Engineering, Qingdao University of Science and Technology, Qingdao 266042, PR China

ARTICLE INFO

Article history:
Received 21 December 2013
Received in revised form
24 February 2014
Accepted 25 February 2014
Available online 18 March 2014

Keywords:
Tumor-associated carbohydrate antigens
Tn antigen
Photoelectrochemical biosensor
Graphene

ABSTRACT

Tumor-associated carbohydrate antigens (TACAs) are often found on the surface of cancer cells. The determination of the carbohydrate components of glycoconjugates is challenging because of the chemical complexity of glycan chains. Through monitoring corresponding antibody, we can get a good solution for clinical diagnosis. Here breast tumor-associated carbohydrate antigens Tn were used as a model and a new photoelectrochemical biosensor for ultrasensitive detection of antibody against Tn was developed. To enhance the sensitivity, both graphene oxide and graphene were used during the construction of biosensor. Through the formation of immunocomplex and the insoluble biocatalytic precipitation (BCP) product, photocurrent intensity was decreased greatly and the antibody could be detected from 0.5 to 500 pg/mL with a detection limit of 1.0×10^{-13} g/mL. At the same time, the developed biosensor showed acceptable selectivity and could be used in the complex matrix. Compared with the traditional glycoarray method, this PEC method is more sensitive (5 orders of magnitude), and thus provides another platform to monitor the immune response to carbohydrate epitopes at different stages during differentiation, metastasis, or treatment.

1. Introduction

The mammalian cell surface is decorated with a dense layer of carbohydrates, which are attached to membrane glycoproteins and glycolipids. Carbohydrate-binding proteins and their glycoconjugate ligands play significant roles in a number of critical biological processes including cell adhesion, signal transduction, immune responses, cell–cell communication, tumor growth and metastasis (He et al., 2011; Liang et al., 2009; Seo et al., 2007). Therefore, sensitive analysis of carbohydrates in various events is keenly desirable for basic science advancement and clinical diagnostics. Malignant transformations resulting in defects in the cellular glycosylation machinery lead to aberrant changes of cell surface carbohydrates and overexpression of TACAs (Sen-itiroh, 1991). Several TACAs have been identified as mediating key pathophysiological events during various steps of cancer progression (Liang et al., 2009). For example, it is recommended that the capping monosaccharide sialic acid has a high metastatic ability in many types of cancers (Schauer, 1985). Terminal glycan epitopes including sialyl Lewis x, Lewis y and Globo H are usually found on transformed cells (Sell, 1990; Taylorpapadimitriou and Epenetos, 1994). The Tn (GalNAcal→*O*-Ser/Thr) (Springer, 1984; Itzkowitz et al., 1989), sialosyl Tn (NeuAc α2→6GalNAc α→*O*-Ser/Thr) (Itzkowitz et al., 1990; Kjeldsen et al., 1988), and T (Gal βl→3GalNAc αl→*O*-Ser/Thr) (Springer, 1984; Itzkowitz et al., 1989) antigens produced by incomplete glycosylation have been well-documented as cancer-related markers and as important antigens for the detection, particularly relevant to breast cancer (Roy et al., 2001). Thus, the glycosylation patterns and glycosylation levels of cells often act as biomarkers to convey information about the physiological state of the cells.

In addition to the chemical complexity of glycan chains, carbohydrates have no natural chromophores or fluorophores, and often show poor ionization efficiency in mass spectrometry (MS). As a result, the determination of the carbohydrate components of glycoconjugates is challenging, which limit the development of glycobiology. So, there are critical needs for developing effective new glycotechnologies and biosensors that are sensitive, rapid, simple, reliable, and cost-effective. At present, the analytical techniques for carbohydrate detection include chromatography, mass spectrometry, and nuclear magnetic resonance (NMR) and surface plasmon resonance (SPR) (Dam and Brewer, 2002; Perou, 2000; Blixt et al., 2008). Usually, these methods examine a single carbohydrate motif, which is tedious, requiring extensive instrumental setup and technical

* Corresponding authors. Tel./fax: +86 532 84022681
E-mail addresses: zhangxr7407@126.com (X. Zhang), qdshyniu@163.com (S. Niu).

http://dx.doi.org/10.1016/j.bios.2014.02.071
0956-5663/

expertise. In addition, many of these assays are also disadvantaged by requirements of extraction and purification steps for modification of glycans structures (Gao et al., 2010). These difficulties can be dissolved by detecting corresponding anti-TACAs antibodies present in the plasma of cancer patients (Huang et al., 2006). Thus, the complex detection for oligosaccharides can be converted to conventional immunoassay.

However, it was reported that carbohydrates tended to bind only weakly to their complementary proteins. Their dissociation constants are in the range of $K_d = 10^{-6}$–10^{-7} M for glycoproteins (Pieters, 2009; Vedala et al., 2011). Stronger binding or enhanced inhibition is often achieved by the use of multiple interactions by multivalent carbohydrates. The most familiar multivalent systems include the small organic compounds of low valency (Liu and Roy, 2001), dendritic systems (Aoi et al., 1995) or linear polymeric systems (Vázquez-Dorbatt et al., 2009). Recently, inorganic platforms have appeared in the literature in the form of glyconanoparticles. These carriers include gold nanoparticles (Fuente et al., 2001), quantum dot (Babu et al., 2007) and single walled carbon naotubes (Gu et al., 2008).

The photoelectrochemical (PEC) detection method is a newly developed and promising analytical method for biological assay. The use of electronic detection makes the PEC instrument simple and low-cost. On the other hand, due to the different forms of energy for excitation (light) and detection (current), this method is very sensitive with low background signals (Zhang et al., 2013; Sun et al., 2013). Now, graphene and QD nanocomposites have been widely investigated in both photovoltaic devices and PEC biosensors (Guo et al., 2010; Zhang et al., 2012; X. Zhao et al., 2012). QDs such as CdS or CdSe QD are usually used photoelectrochemically active species, while graphene which has large donor/acceptor interfaces for charge generation and a continuous pathway for electron transfer can act as an efficient acceptor to improve the PEC performance of QDs. Here we use graphene/CdSe nanocomposite as a sensitive photoelectric interface. It should be noted that CdSe QD used here acted as both photosensitizer and an alternative multivalent presentation form for carbohydrate antigen with high binding affinity. To improve the sensitivity further, horseradish peroxidase (HRP) catalyzed biocatalytic precipitation (BCP), which was first introduced to PEC biosensor by Xu's group (Zhao et al., 2012a, 2012b), was also applied using functionalized graphene oxide (GO) as a nanocarrier for HRP. Simple glycoantigen Tn and Tn specific IgM antibody were used as a model for investigating the interaction between carbohydrate and protein. The principle of the sensing design is shown in Scheme 1. This design will facilitate testing for disease-related sugar markers as well as evaluate the immunogenic properties of carbohydrate vaccine candidates.

2. Experimental

2.1. Materials and chemicals

2.1.1. Materials

Graphite powder, $NaNO_3$, $KMnO_4$, selenium power, $CdCl_2$, $NaBH_4$, Tween 20, hydrazine monohydrate, $ClCH_2COONa$ and ascorbic acid (AA) were all of analytical grade and obtained from Sinopharm Chemical Reagent Co., Ltd. Tn Epitope (Tn), 4-chloro-1-naphthol, N-(3-dimethylaminopropyl)-N-ethyl-carbodiimide hydrochloride (EDC) and N-hydroxysuccinimide (NHS) were purchased from J&K chemical (China). Goat anti-mouse IgM (Ab_2), and HRP-labeled goat anti-mouse IgM (HRP-Ab_2) were obtained from Boisynthesis Biotechnology co., Ltd. (Beijing, China). Tn Antigen monoclonal antibody was purchased from Thermo Scientific. Poly(diallyldimethylammonium chloride) (PDDA; 20%, w/w in water, MW = 200,000–350,000), bovine serum albumin (BSA), and thioglycolic acid (TGA) were purchased from Sigma-Aldrich (St. Louis, MO). Other chemicals were of analytical reagent grade and used as received. PBS (0.01 M, pH 7.4) was used for the preparation of Tn and Ab solutions. All aqueous solutions were prepared using ultrapure water (Milli-Q, Millipore).

To prepared 4-chloro-1-naphthol stock solution, 4-chloro-1-naphthol was initially dissolved in ethanol, and then 1 mL ethanolic stock solution (0.05 M) was diluted with 0.1 M phosphate buffer (pH 7.4) to 50 mL.

2.1.2. Apparatus

The photocurrent was measured on an electrochemical workstation (Zahner Zennium, Germany). A three-electrode system was employed with Pt wire as an auxiliary electrode, Ag/AgCl as a reference electrode and ITO conductive glass supplied by Weiguang Corp. (Shenzhen, PR China, ITO coating 180 ± 25 nm, sheet resistance $\leq 10\ \Omega$/square) as a working electrode. Scanning electron microscopy (SEM) (JSM-6700F, JEOL, Japan) was used to examine the morphology of modified electrodes. UV/vis spectra were carried out on a Cary 50 UV/Vis–NIR spectrophotometer (Varian). Raman measurements were conducted on an inVia Raman Microscope (Renishaw, England).

2.2. Synthesis of graphene oxide (GO)

Graphene oxide was synthesized from natural graphite by a modified Hummers method (Hummers and Offeman, 1958; K. Zhang et al., 2010). Graphite (5 g) and $NaNO_3$ (2.5 g) were mixed with 120 mL of H_2SO_4 (95%) in a 500 mL flask. The mixture

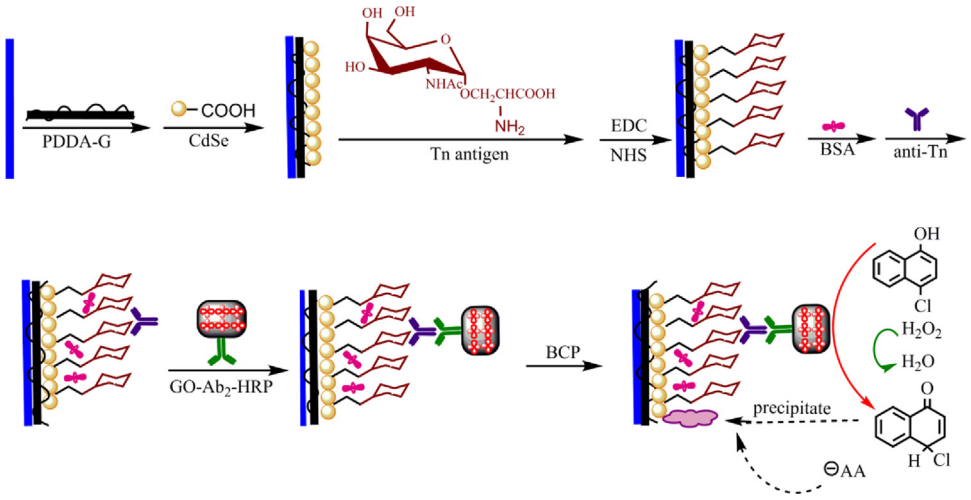

Scheme 1. Schematic diagram of the stepwise immunosensor fabrication process.

was stirred for 30 min within an ice bath. Then potassium permanganate (15 g) was added to the suspension and the mixture was stirred at room temperature overnight. 150 mL of H_2O was slowly added to the mixture with vigorous agitation and the diluted suspension was stirred at 98 °C for one day. Subsequently, 50 mL of 30% H_2O_2 was added to the mixture and the color changed to brown and yellow. For purification, the mixture was washed by rinsing and centrifugation with 5% HCl and then double distilled water (DDW) for several times. After filtration and drying under vacuum, the graphene oxide (GO) was obtained as a gray powder.

2.3. Synthesis of PDDA-functionalized graphene (PDDA–G)

PDDA-functionalized graphene was prepared according to the reported method (Liu et al., 2010). To 100 mL 0.5 mg/mL GO, 5 mL PDDA (20%) solution was added and ultrasonicated for 30 min. The resulting mixture was further treated with 0.5 mL hydrazine hydrate (80%) and allowed to react for 24 h at 90 °C. Finally, the black PDDA-functionalized graphene (PDDA–G) was collected by filtration and further washed with water to remove the excess hydrazine.

2.4. Synthesis of carboxylated GO (GO-COOH)

For synthesis of carboxylated GO (Du et al., 2011), GO aqueous suspension (1 mg/mL) was bath sonicated for 1 h to give a clear solution. Then, 200 mg of NaOH and 200 mg of $ClCH_2COONa$ were added to 4 mL of 1 mg/mL GO solution obtained above, followed by bath sonication for 2 h. The resulting product was neutralized with dilute hydrochloric acid and purified by repeated rinsing and centrifugation until the product was well dispersed in DDW. After dialyzed against DDW for 48 h, the solution of GO-COOH was obtained.

2.5. Preparation of GO–Ab2–HRP conjugate

For synthesis of GO–Ab_2–HRP conjugate (Du et al., 2011), HRP and Ab_2 were attached to GO-COOH by using the classic coupling reactions between –COOH groups on the surfaces of GO-COOH and the $–NH_2$ groups of protein. Briefly, 1 mL of 1.0 mg/mL GO-COOH was mixed with 150 μL of 2 mmol/L NHS and 150 μL of 8 mmol/L EDC and activated for 30 min. The mixture was centrifuged at 10,000 rpm for 30 min, and the supernatant was discarded. The buffer wash was repeated to remove excess EDC and NHS. Subsequently, the resulting functionalized mixture was dispersed in 1.0 mL of pH 7.4 PBS and sonicated for 5 min to obtain a homogeneous dispersion. Then, 2 μL of HRP (7.5×10^{-3} g/mL) and 2 μL Ab_2 (5.0×10^{-5} g/mL) were added to the dispersion, and the mixture was incubated in a shaking water bath at room temperature. After stirred overnight at 4 °C, the reaction mixture was washed three times with PBS and centrifuged at 10,000 rpm for 30 min. The supernatant was discarded and the precipitation was redispersed in 1.0 mL of pH 7.4 PBS containing 1% BSA and centrifuged at 10,000 rpm for 30 min again to remove the excess BSA. Finally, redispersed the resulting product in 1.0 m L of pH 7.4 PBS and stored at 4 °C for later use.

2.6. Immunosensor construction and enzymatic biocatalytic precipitation (BCP)

Briefly, the ITO slices were sonicated in acetone, NaOH (1 M) in 1:1 (v/v) ethanol/water and water, respectively, for about 15 min each, followed by drying in the oven for later use. 10 μL of 5 mg/mL PDDA–G was casted on the cleaned ITO slices and incubated at room temperature for 40 min. Then 10 μL CdSe-COOH NPs (synthesized in Supplementary materials) was casted on and incubated at room temperature for 2 h to give photoelectrochemical active interface. Following this step, the electrode was activated by 0.2 M EDC and 0.1 M NHS for 30 min. Then 10 μL of 1.0×10^{-3} M Tn antigen was dropped on the electrode surface and the electrode was incubated at room temperature for 2 h. After blocking with 10 μL of 2% BSA for 2 h, 10 μL of analyte (Tn Antibody) with different concentrations were added and the mixture was incubated at 37 °C for 1.5 h. Finally, 10 μL of 3.0×10^{-5} g/mL Ab_2–HRP or GO–Ab_2–HRP prepared above was casted on and incubated at 37 °C for 1 h.

The electrode surface was rinsed with washing buffer (0.01 M PBS containing 0.05% Tween 20) and DDW, then dried under nitrogen atmosphere after each step of the fabrication process in order to remove nonspecific adsorption.

During the BCP reaction, the modified electrode was incubated with an analyte solution consisting of 1.0×10^{-3} M 4-chloro-1-naphthol and 1.5×10^{-4} M H_2O_2 for 10 min. Thereafter, the electrode was introduced for PEC measurement.

2.7. PEC detection

Photoelectrochemical detection was carried out in 0.1 M PBS (pH = 7.4) containing 0.1 M ascorbic acid (AA) which was served as a sacrificial electron donor during the photocurrent measurement. Light excitation of 430 nm was switched every 10 s.

3. Results and discussion

3.1. SEM image of ITO electrode at different modification processes

To confirm the successful assembly on ITO electrode at different modification processes, SEM images were performed. Fig. 1A is a typical SEM image of PDDA-functionalized graphene (PDDA–G) modified ITO surface, showing that the functionized graphene had a sheet-like morphology with a clear, smooth surface. Fig. 1B shows the SEM image of the surface after the attachment of the CdSe NPs, which were uniformly distributed on graphene. From TEM shown in Fig. S1 (see Supplementary material), we could also see that CdSe-COOH NPs were assembled on the surface of graphene successfully. Fig. 1C reveals the SEM image of the electrode surface after covalent immobilization of Tn antigen, recognition with anti-Tn and GO–Ab_2–HRP conjugate. Then, after BCP on the electrode surface, distinctive difference in the topography was found in Fig. 1D. The inserted Fig. 1E is the amplification of Fig. 1D. From the image changes shown in Fig. 1, we could see the well-behaved assembly process.

3.2. Preparation of GO conjugate and its UV–visible spectra

In recent years, functional graphene oxide (GO) has been extensively investigated as a nanocarrier (Liu et al., 2008; L. Zhang et al., 2010). In order to facilitate the binding of enzymes and antibodies to GO as well as increase water solubility, it is necessary to convert ester, hydroxyl, and epoxide groups in the GO sheets into carboxyl groups. According to the literature (Fan et al., 2008; Dai et al., 2006), we activated the GO with $ClCH_2COONa$ under strongly basic conditions. After neutralization, wash and dialysis, the precipitated GO-COOH was dispersed in water (Fig. 2A). During this process, the color of the GO suspension changed from brown to black, which is probably due to partial reduction of the GO under strong alkaline conditions.

HRP and Ab_2 were attached to GO-COOH using classic EDC/NHS amidization protocol. The resulting GO–Ab_2–HRP composite was further characterized by UV–vis spectroscopy. As shown in Fig. 2B,

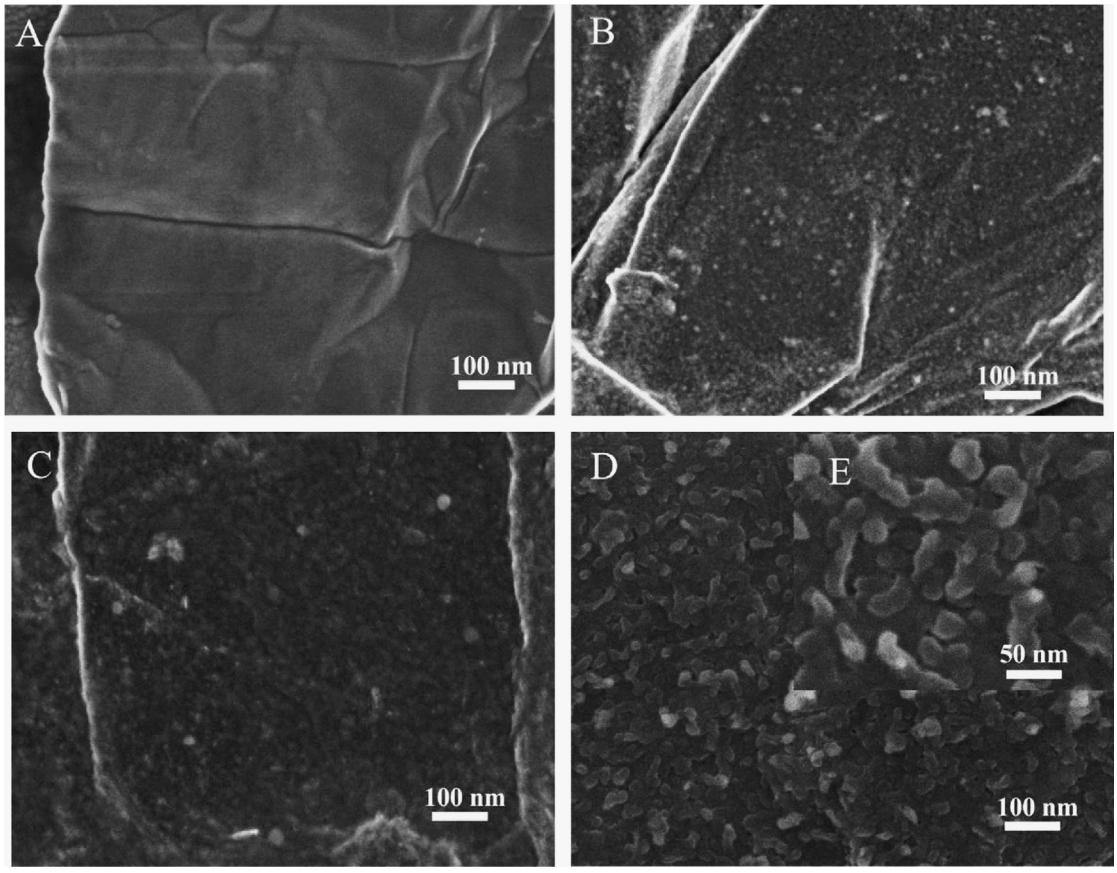

Fig. 1. SEM images of ITO electrode after modification of (A) PDDA–G, (B) G–CdSe composite film, (C) G–CdSe-(GO–Ab_2–HRP), (D) and (E) electrode of (C) after BCP. Scale bars = 100 nm for (A), (B), (C) and (D), 50 nm for (E).

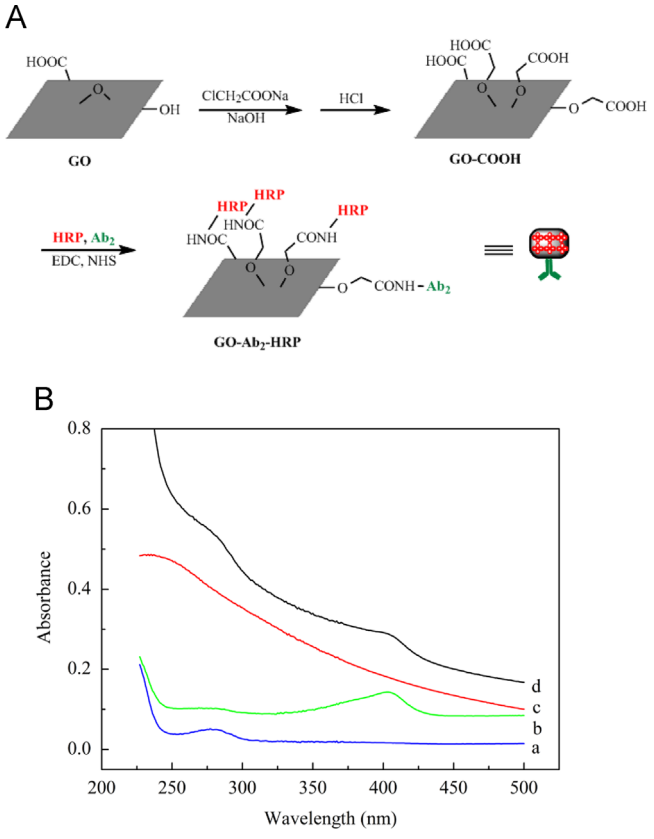

Fig. 2. (A) The carbonylation of GO surface and preparation of GO–Ab_2–HRP conjugate; (B) UV–vis spectra of (a) Ab_2 (b) HRP (c) GO-COOH and (d) GO–Ab_2–HRP.

there was no absorption peak for the GO-COOH (curve c). The absorptions of Ab_2 and HRP were observed at 277 nm (curve a) and 403 nm (curve b) respectively. As for GO–Ab_2–HRP conjugate, there were two obvious absorption peaks (curve d). These proved that Ab_2 and HRP had been successfully bound to GO.

3.3. Raman Spectra of graphene derivates

The Raman spectra of GO, GO-COOH and PDDA–G are shown in Fig. S2 (see Supplementary material). Two obvious bands located at around 1580 cm^{-1} and 1350 cm^{-1} were observed in the Raman spectra, which were generally assigned as the G band and D band, respectively. By comparing the intensity of the G and D bands, we could speculate the information about the disordered and ordered crystal structures of carbon. The value of I(D)/I(G) for GO was 1.75, suggesting many disorders in the structure of GO. The value of I(D)/I(G) for PDDA–G (1.39) was smaller than that of GO due to the orders of graphene were partly recovered along with the reduction. The value of I(D)/I(G) for G-COOH (1.56) was smaller than that of GO but bigger than that of PDDA–G, suggesting partial reduction of the GO under strong alkaline conditions as described above.

3.4. Amplification of GO as a nanocarrier

Furthermore, we investigated the amplification effect of GO as a nanocarrier. As shown in Fig. 3A and B, when HRP labeled Ab_2 (Ab_2-HRP) was used during the sandwich immunoreactions, the photocurrent decreased from 5.8 μA to 5.1 μA after BCP reaction using 100 pg mL^{-1} anti-Tn. While, when GO–Ab_2–HRP conjugate was used instead, the photocurrent decreased to 1.8 μA with the same concentration of anti-Tn. The achieved amplification of

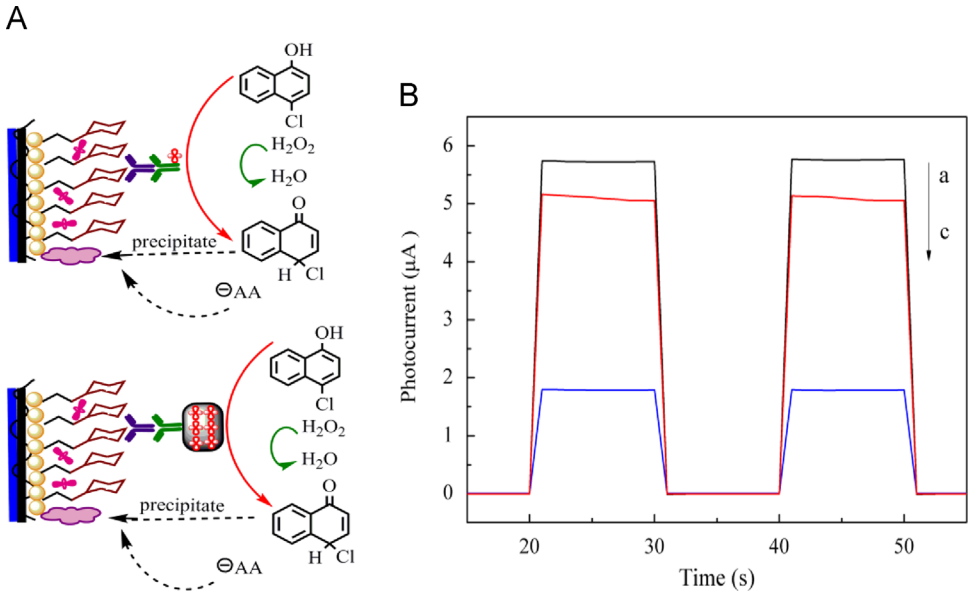

Fig. 3. (A) HRP-catalyzed BCP format with and without the amplification of GO. (B) Photocurrent responses for (a) ITO/PDDA–G/CdSe/Tn/BSA; (b) ITO/PDDA–G/CdSe/Tn/BSA/100 pg mL^{-1} antiTn/HRP-Ab_2/BCP; and (c) ITO/PDDA–G/CdSe/Tn/BSA/100 pg mL^{-1} antiTn/ HRP–Ab_2–GO/BCP.

signal was ascribed to a large amount of HRP loaded on the GO nanocarrier.

3.5. Ratio optimization for HRP and Ab_2 assembled on GO

Since HRP rather than Ab_2 could amplify photoelectronical detection, the number of HRP on the surface of nanoparticles should reach saturation while the number of Ab_2 should keep a minimum. However, low concentration of Ab_2 may decrease immunocoupling efficiency on the electrode surface, which may result in a decreased response. So the ratio of HRP to Ab_2 should be optimized in order to provide maximum signals. As shown in Fig. S3 (see Supplementary material), the photocurrent increased with increasing the ratio of HRP/Ab_2, and the maximum response was achieved at the ratio of 150/1. Therefore, the HRP/Ab_2 ratio of 150/1 was selected as the optimal condition to prepare the GO–Ab_2–HRP composite.

3.6. Amplification effect of graphene during the construction of photosensitive interface

Amplification effect of graphene on photocurrent is shown in Fig. S4 (see Supplementary material). No photoresponse was observed at graphene modified ITO because graphene could not be excited (curve c). QDs sensitized graphene photoelectrode generated photocurrent at about 6.6 μA (curve a). Under the same condition, the photocurrent for pure CdSe QDs modified ITO electrode was only about 2.5 μA. (curve b). This may be explained that graphene has large donor/acceptor interfaces for charge generation and a continuous pathway for electron transfer, thereby effectively impeding the charge recombination of excited CdSe QDs, and resulting in a much more sensitive response.

3.7. Photoresponse of assembled photosensitive interface

It is also worth mentioning that the photoresponse process of this nanocomposite is rapid under ON/OFF switching. Meanwhile, no apparent photocurrent degradation is observed up to 12 cycles (Fig. S5, see Supplementary material). These observations suggest that the obtained nanocomposite provides excellent charge dissociation and transportation. The stable character makes it to be used as a detection signal.

3.8. Microgravimetric quartz crystal microbalance measurements

Quartz crystal microbalance (QCM) biosensor format has been increasingly adopted due to its convenient means of operation coupled with high performance. Here we use QCM to estimate the maximum amount of antibody assembled on the platform. The assemble process for PDDA–G, CdSe QDs and Tn antigen on the gold surfaces of QCM crystals was the same as that on ITO electrode. After blocked by 300 μL of 2% BSA for 30 min, 300 μL of 3.0×10^{-5} g/mL anti-Tn was injected and the changes in frequency of the QCM were monitored. From the changes in the crystal frequencies, we estimated the maximum surface coverage of anti-Tn to be 1000 ng/cm^2 (Fig. S6, see Supplementary material).

3.9. Fabrication process of biosensor

Electrochemical impedance spectroscopy (EIS) is a valuable and effective tool to characterize surface modifications and detect bior-ecognition processes. As shown in Fig. S7 (see Supplementary material), for a bare ITO electrode surface, the impedance spectrum (curve a) exhibited a small semicircle. After the adsorption of PDDA/G and CdSe NPs, the Ret increased progressively. This increase in diameter indicated that the charge transfer rate of $[Fe(CN)_6]^{4-/3-}$ was reduced gradually, which was attributed to the hindrance effect to this redox couple caused by the deposition of PDDA–G/CdSe on the electrode surface. When small molecule Tn antigen was covalently immobilized on the electrode surface, the resistance Ret increased slightly (curve d). When blocked with BSA, the Ret further increased (curve e). After specific immunoreaction between antibody and antigen, and subsequent immobilization of GO–Ab_2–HRP composite, the Ret increased gradually as the experiment proceeds (curves f–g). These were consistent with the fact that the layer of protein molecules could insulate the conductive support and perturb the interfacial electron transfer between the electrode and the electroactive species in solution. In the final step, after BCP reaction, the Ret increased greatly due to the insoluble precipitation layer produced by BCP reaction obstructed the mass transport and electron transfer of the electrochemical probe to the electrode surface.

In order to characterize the fabrication process of the photoelectrochemical biosensor, photocurrent responses at each immobilization step were recorded. As shown in Fig. 4A, the photocurrent for PDDA–G/CdSe composite modified ITO electrode was about 6.56 nA (curve a). When Tn antigen was covalently attached on the –COOH groups of CdSe NPs (curve b) and blocked with BSA (curve c), the photocurrent decreased slightly. Then the photocurrent decreased obviously after recognition with 500 pg mL^{-1} anti-Tn (curve d) and HRP–Ab_2–GO composite (curve e). The formation of Ag–Ab_1 and Ag–Ab_1–Ab_2–GO–HRP sandwich immunocomplexes would greatly increase the steric hindrance and hence retard the diffusion of the solubilized electron donor (AA) to the surface of the underlying CdSe QDs film. Finally, after enzymatic biocatalytic precipitation, the formation of insoluble and insulating product by BCP would thereby introduce an isolating barrier for the electron-transfer at the electrode interface and lead to further decrease of photocurrent (curve f). Through multiple amplification steps, target anti-Tn could be detected sensitively.

3.10. Sensitivity and selectivity

The quantitative behavior of the photoelectrochemical immunoassay was assessed by measuring the dependence of the photocurrent decrement when incubated with different concentrations of anti-Tn. Fig. 4B shows that the photocurrent signals were responsive to the changing concentrations of anti-Tn (a–h). The photocurrent intensity gradually decreased with increasing anti-Tn concentrations. As shown in Fig. 4C, the decrease of photocurrent intensity was linearly related to the logarithm of the anti-Tn concentrations in a linear range from 0.5 to 500 pg mL^{-1}. The regression equation was ΔI (μA)=0.13+0.26lgC (pg mL^{-1}) with a regression coefficient of 0.9946. A detection limit of 1.0×10^{-13} g mL^{-1} could be estimated using 3σ. With the amplification of GO, the sensitivity of the proposed method was enhanced about 200-fold compared to a simple photoelectrochemical detection based on HRP labeled Ab_2 (Ab_2-HRP) (see Figs. S8 and S9 in Supplementary materials). In addition, compared with the report of Wong's group, who applied glycan microarray assay for the detection of corresponding antibodies, the sensitivity of our technique was more sensitive (5 orders of magnitude) (Huang et al., 2006). It should be pointed out that carbohydrate antigens assembled on QDs can mimic the multiple glycan expressed on cell surface and thus meet the requirements for multivalent interaction to a certain degree.

Control experiments revealed the photocurrent responses when incubated with 500 pg/mL of foreign proteins, such as

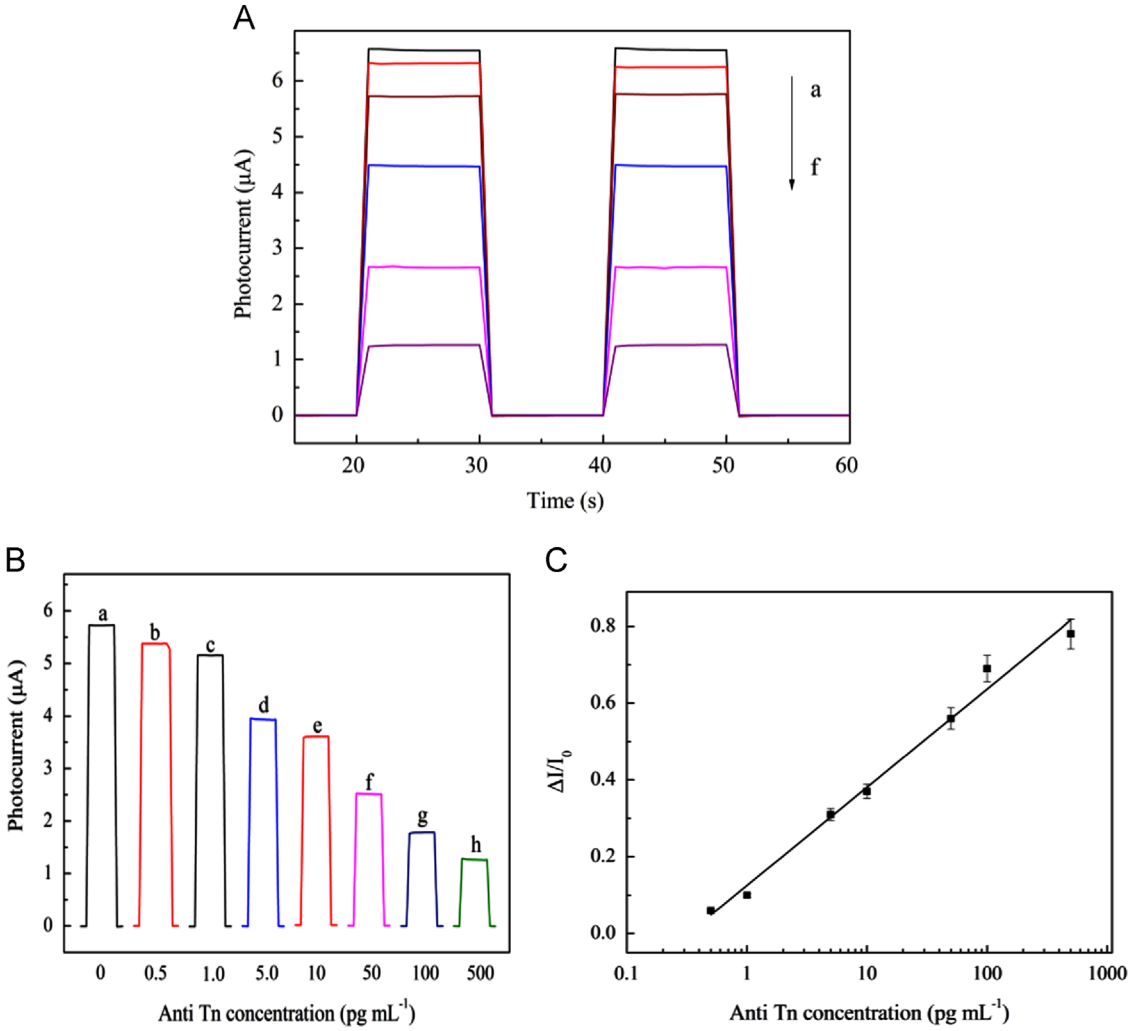

Fig. 4. (A) Photocurrent responses for (a) ITO/PDDA–G/CdSe; (b) ITO/PDDA–G/CdSe/Tn; (c) ITO/PDDA–G/CdSe/Tn/BSA; (d) ITO/PDDA–G/CdSe/Tn/BSA/500 pg mL^{-1} anti Tn; (e) ITO/ PDDA–G/CdSe/Tn/BSA/500 pg mL^{-1}anti Tn/HRP–Ab_2–GO; and (f) ITO/PDDA–G/CdSe/Tn/BSA/500 pg mL^{-1} anti Tn/HRP–Ab_2–GO/BCP. (B) Photocurrent responses for different concentrations of antibody (a) 0, (b) 0.5, (c) 1.0, (d) 5.0, (e) 10, (f) 50, (g) 100, and (h) 500 pg mL^{-1}. (C) Calibration curve corresponding to the analysis of different concentrations of anti Tn from 0.5 to 500 pg mL^{-1}. $\Delta I=I_0-I$, I_0 was the photocurrent of the modified electrode prior to anti Tn immobilization and I was the final photocurrent of the electrode after BCP.

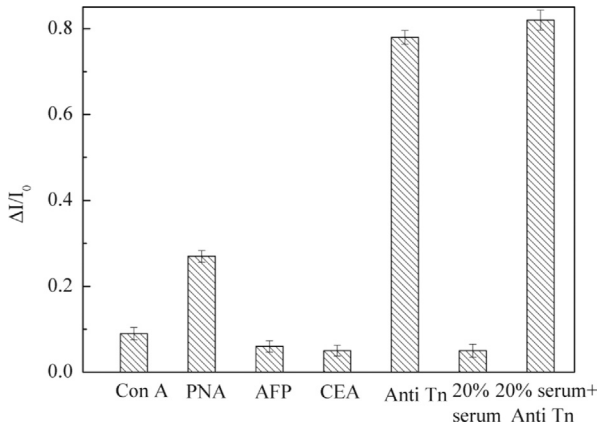

Fig. 5. Selectivity toward different analytes and detection in complex matrixes.

concanavilin A (ConA), peanut agglutinin (PNA), alphafetoprotein (AFP), carcinoembryonic antigen (CEA) and Tn antibody (Fig. 5). Comparing two plant lectins, the photocurrent changes caused by adding PNA was bigger than that of ConA. This could be explained by the recognition effect between GalNAc and PNA. In addition, the photocurrent responses for AFP or CEA were much lower than that of anti Tn, indicating good selectivity caused by specific immunobinding. When spiked 500 pg/mL Tn antibody into 20% serum, the obtained signal had no apparent difference compared to equal amount of Tn antibody in buffer. The ability to detect the analytes in complex matrixes demonstrates the potentialities for medical sensing investigations.

4. Conclusions

In this study, we showed that the developed PEC biosensor could be used for quantitative analysis of monoclonal antibodies anti-Tn, which was used against the breast tumor-associated carbohydrate antigen Tn, with the sensitivity down to 1.0×10^{-13} g/mL level. Several advantages of our method have been demonstrated: (1) to enhance the sensitivity, two graphene derivates were applied. GO was selected as a nanocarrier for more enzyme loading, while PDDA–graphene nanocomposite was used to prepared sensitive photosensitive interface. (2) Multi-signal enhancement including Tn/AntiTn/HRP–Ab_2–GO immunocomplexes and the formation of insoluble product by BCP reaction had introduced isolating barriers for the electron-transfer at the electrode interface and hence retarded the diffusion of donor molecules to the surface of the underlying CdSe QDs film. (3) To the best of our knowledge, this is the first PEC biosensor used for the detection of antibody against tumor-associated carbohydrate antigen. At the same time, it provides a new platform for monitoring the immune response to carbohydrate epitopes after vaccine therapy or during the course of cancer progression.

Acknowledgments

This work was supported by Open Research Fund Program of Key Laboratory of Marine Drugs (Ocean University of China), Ministry of Education of People's Republic of China (KLMD(OUC)201206), the National Natural Science Foundation of China (Nos. 21275003, 21025523, and 21075073), Excellent Young Scientists Encouragement Foundation of Shandong Province (No. BS2011CL015), the Program for Changjiang Scholars and Innovative Research Team in University (PCSIRT).

Appendix A. Supplementary materials

Supplementary data associated with this article can be found in the online version at http://dx.doi.org/10.1016/j.bios.2014.02.071.

References

Aoi, K., Itoh, K., Okada, M., 1995. Macromolecules 28, 5391–5393.
Babu, P., Sinha, S., Surolia, A., 2007. Bioconjugate Chem. 18, 146–151.
Blixt, O., Han, S., Liao, L., Zeng, Y., Hoffmann, J., Futakawa, S., Paulson, J.C., 2008. J. Am. Chem. Soc. 130, 6680–6681.
Dai, Z., Kawde, A., Xiang, Y., Belle, J.T.L., Gerlach, J., Bhavanandan, V.P., Joshi, L., Wang, J., 2006. J. Am. Chem. Soc. 128, 10018–10019.
Dam, T.K., Brewer, C.F., 2002. Chem. Rev. 102, 387–430.
Du, D., Wang, L., Shao, Y., Wang, J., Engelhard, M.H., Lin, Y., 2011. Anal. Chem. 83, 746–752.
Fan, X., Peng, W., Li, Y., Li, X., Wang, S., Zhang, G., Zhang, F., 2008. Adv. Mater. 20, 4490–4493.
Fuente, J.M., Barrientos, A.G., Rojas, T.C., Rojo, J., Cañada, J., Fernández, A., Penadés, S., 2001. Angew. Chem. Int. Ed. 40, 2257–2261.
Gao, J., Liu, D., Wang, Z., 2010. Anal. Chem. 82, 9240–9247.
Gu, L., Luo, P.G., Wang, H., Meziani, M.J., Lin, Y., Veca, L.M., Cao, L., Lu, F., Wang, X., Quinn, R.A., Wang, W., Zhang, P., Lacher, S., Sun, Y.P., 2008. Biomacromolecules 9, 2408–2418.
Guo, C.X., Yang, H.B., Sheng, Z.M., Lu, Z.S., Song, Q.L., Li, C.M., 2010. Angew. Chem. Int. Ed. 49, 3014–3017.
He, X., Wang, X., Jin, X., Zhou, H., Shi, X., Chen, G., Long, Y., 2011. J. Am. Chem. Soc. 133, 3649–3657.
Huang, C., Thayer, D.A., Chang, A.Y., Best, M.D., Hoffmann, J., Head, S., Wong, C., 2006. Proc. Natl. Acad. Sci. USA 103, 15–20.
Hummers, W.S., Offeman, R.E., 1958. J. Am. Chem. Soc. 80, 1339.
Itzkowitz, S.H., Yuan, M., Montgomery, C.K., Kjeldsen, T., Takahashi, H.K., Bigbee, W. L., Kim, Y.S., 1989. Cancer Res. 49, 197–204.
Itzkowitz, S.H., Bloom, E.J., Kokal, W.A., Modin, G., Hakomori, S., Kim, Y.S., 1990. Cancer 66, 1960–1966.
Kjeldsen, T., Clausen, H., Hirohashi, S., Ogawa, T., Iijima, H., Hakomori, S., 1988. Cancer Res. 48, 2214–2220.
Liang, C., Wang, C., Lin, Y., Chen, C., Wong, C., Wu, C., 2009. Anal. Chem. 81, 7750–7756.
Liu, B., Roy, R., 2001. Tetrahedron 57, 6909–6913.
Liu, K., Zhang, J., Yang, G., Wang, C., Zhu, J., 2010. Electrochem. Commun. 12, 402–405.
Liu, Z., Robinson, J.T., Sun, X.M., Dai, H.J., 2008. J. Am. Chem. Soc. 130, 10876–10877.
Perou, C.M., 2000. Nature 406, 747–752.
Pieters, R.J., 2009. Org. Biomol. Chem. 7, 2013–2025.
Roy, R., Baek, M., Rittenhouse-Olson, K., 2001. J. Am. Chem. Soc. 123, 1809–1816.
Schauer, R., 1985. Trends Biochem. Sci. 10, 357–360.
Sell, S., 1990. Hum. Pathol. 21, 1003–1019.
Sen-itiroh, H., 1991. Curr. Opin. Immunol. 3, 646–653.
Seo, J.H., Adachi, K., Lee, B.K., Kang, D.G., Kim, Y.K., Kim, K.R., Lee, H.Y., Kawai, T., Cha, H.J., 2007. Bioconjugate Chem. 18, 2197–2201.
Springer, G.F., 1984. Science 224, 1198–1206.
Sun, B., Zhang, K., Chen, L., Guo, L., Ai, S., 2013. Biosens. Bioelectron. 44, 48–51.
Taylorpapadimitriou, J., Epenetos, A.A., 1994. Trends Biotechnol. 12, 227–233.
Vázquez-Dorbatt, V., Tolstyka, Z.P., Chang, C., Maynard, H.D., 2009. Biomacromolecules 10, 2207–2212.
Vedala, H., Chen, Y., Cecioni, S., Imberty, A., Vidal, S., Star, A., 2011. Nano Lett. 11, 170–175.
Zhang, K., Zhang, L., Zhao, X., Wu, J., 2010. Chem. Mater. 22, 1392–1401.
Zhang, L., Xia, J., Zhao, Q., Liu, L., Zhang, Z., 2010. Small 6, 537–544.
Zhang, X.R., Guo, Y.S., Liu, M.S., Zhang, S.S., 2013. RSC Adv. 3, 2846–2857.
Zhang, X., Xu, Y., Yang, Y., Jin, X., Ye, S., Zhang, S., Jiang, L., 2012. Chem. Eur. J 18, 16411–16418.
Zhao, X., Zhou, S., Jiang, L., Hou, W., Shen, Q., Zhu, J., 2012. Chem. Eur. J. 18, 4974–4981.
Zhao, W., Ma, Z., Yu, P., Dong, X., Xu, J., Chen, H., 2012a. Anal. Chem. 84, 917–923.
Zhao, W., Dong, X., Wang, J., Kong, F., Xu, J., Chen, H., 2012b. Chem. Commun. 48, 5253–5255.